Unconventional London Penetration Depth in Single-Crystal $Ba(Fe_{0.93}Co_{0.07})_2As_2$ Superconductors

R. T. Gordon, N. Ni, C. Martin, M. A. Tanatar, M. D. Vannette, H. Kim, G. D. Samolyuk, J. Schmalian, S. Nandi, A. Kreyssig, A. I. Goldman, J. Q. Yan, S. L. Bud'ko, P. C. Canfield, and R. Prozorov*

Ames Laboratory and Department of Physics and Astronomy, Iowa State University, Ames, Iowa 50011, USA

(Received 13 October 2008; published 26 March 2009)

The London penetration depth $\lambda(T)$ has been measured in single crystals of $Ba(Fe_{0.93}Co_{0.07})_2As_2$. The observed low-temperature variation of $\lambda(T)$ follows a power law, $\Delta\lambda(T) \sim T^n$ with $n \approx 2.4 \pm 0.1$, indicating the existence of normal quasiparticles down to at least $0.02T_c$. This is in contrast with previous penetration depth measurements on single crystals of $NdFeAsO_{1-x}F_x$ and $SmFeAsO_{1-x}F_x$, which indicate an anisotropic but nodeless gap. We discuss possible explanations of the observed power law behavior.

DOI: 10.1103/PhysRevLett.102.127004 PACS numbers: 74.25.Nf, 74.20.Mn, 74.20.Rp

The discovery of superconductivity in $LaFeAs(O_{1-x}F_x)$, with $T_c \approx 23$ K [1], and T_c above 50 K in $SmFeAs(O_{1-x}F_x)$ [2], has led to a flurry of activity aimed at understanding the fundamental physics governing this new family of superconductors. Much effort has been put forth to characterize the oxypnictide compounds $RFeAsO_{1-x}F_y$ (R = rare earth, denoted "1111"), as well as oxygen-free $A(Fe_{1-x}T_x)_2As_2$ (A = alkaline earth and T = transition metal, denoted "122"). The major questions yet to be answered are the symmetry of the superconducting gap and its universality among all Fe-based pnictides. High T_c, high upper critical fields, and the existence of a unique structural element, Fe-As layers, prompt a comparison with the high-T_c cuprates.

The unique feature of the cuprates is d-wave symmetry of the order parameter (OP) [3]. In the Fe-based pnictides the debate is wide open and different scenarios are discussed, including gapped versus nodal, or single versus multigap superconductivity. Tunneling shows an unconventional OP with nodes [4], two superconducting gaps, and a pseudogap [5], as well as conventional s-wave BCS behavior [6]. Specific heat has also shown both conventional [7] and unconventional [8] behavior. Angle-resolved photoemission data are still in disagreement regarding the gap(s) structure and amplitude [9,10].

With respect to the penetration depth, $\lambda(T)$, microwave cavity perturbation in $PrFeAsO_{1-x}$ [11] and muon spin relaxation (μSR) in both $LaFeAsO_{1-x}$ [12] and $SmFeAsO_{1-x}F_x$ [13] concluded a nodeless OP. Single-crystal measurements in $SmFeAsO_{1-x}F_x$ [14] and $NdFeAsO_{1-x}F_x$ [15] have found exponential behavior of $\lambda(T)$. However, magnetism of rare-earth ions may significantly affect these observations as had happened with electron-doped cuprates [16]. In the 122 iron pnictides the question of the OP symmetry is still open. Until now much attention has been devoted to the cuprates, where the band structure is essentially two dimensional and line nodes in the gap result in a $\lambda(T) \sim T$ behavior in the clean limit [3], changing to $\sim T^2$ with impurities [17]. Still, other materials may have nodes in a three-dimensional gap. There is evidence for point nodes in the heavy fermion $PrOs_4Sb_{12}$ [18,19] and possibly the nonmagnetic borocarbides [20].

In this Letter, we focus on the $Ba(Fe_{0.93}Co_{0.07})_2As_2$ member of the 122 family, for which high quality single crystals are available [21–23]. Its behavior in the mixed state is similar to the high-T_c cuprates [23], and so one could expect to find unconventional behavior in other properties as well.

Single crystals of superconducting $Ba(Fe_{1-x}Co_x)_2As_2$ were grown out of Fe-As flux using standard high-temperature solution growth techniques [24,25]. The crystal dimensions can be as large as $12 \times 8 \times 1$ mm^3. Elemental analysis has shown that the actual Co concentration, averaged over six measurements, is $Co/(Co + Fe) = 7.4\% \pm 0.2\%$. Doping at this level completely suppresses the antiferromagnetism and orthorhombic structural distortion, typical for the parent compound. Crystals selected from several different batches have been characterized by various techniques. Powder x-ray diffraction on ground crystals has yielded tetragonal lattice constants of $a = 3.9609 \pm 0.0008$ Å and $c = 12.9763 \pm 0.004$ Å. Single-crystal x-ray diffraction measurements have found no evidence of a tetragonal-to-orthorhombic structural transition [Figs. 1(a) and 1(b)]. In particular, the orthorhombic splitting observed in $(\nu\ \nu\ 0)$ scans for the parent compound [24] with a value of $\Delta\nu \sim 0.005$ at 10 K should be clearly observable as illustrated by the arrows in Fig. 1(b). Furthermore, the similarity of the diffraction peak widths for the Co-doped and the parent $BaFe_2As_2$ compound indicates that the Co doping is homogeneous. Figure 1(c) shows the T-dependent in-plane resistivity, dc magnetization, and penetration depth. T_c, as defined by zero resistivity, coincides with the onset of diamagnetic magnetization and is close to the beginning of a sharp decrease in $\lambda(T)$.

Measurements of the London penetration depth, $\lambda(T)$, were performed using a tunnel diode resonator technique [26–28]. A properly biased tunnel diode acts as an ac power source for the LC circuit that promotes spontaneous

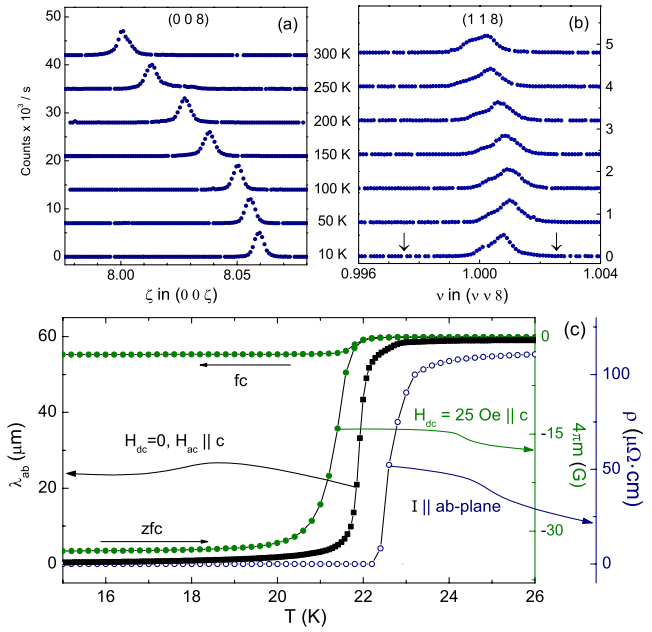

FIG. 1 (color online). Characterization of $Ba(Fe_{1-x}Co_x)_2As_2$ single crystals. (a) Longitudinal x-ray scans through the position of the (0 0 8) reflection for indicated temperatures. (b) Transverse (ν ν 0) scans through the position of the (1 1 8) reflection. Changes in the position of the peaks in (a) and (b) result from thermal expansion of the lattice. The asymmetric peak shape in the (ν ν 0) scan originates from a second grain with a slightly different orientation (sample mosaic) and is present at all temperatures. In (a) and (b) the horizontal axes depict the reciprocal lattice vectors relative to the alignment and lattice parameters at 300 K. The vertical arrows in (b) depict the positions of the split diffraction peaks at 10 K in the parent $BaFe_2As_2$ compound (after Ref. [24]). (c) In-plane resistivity (open circles), dc magnetization (filled circles), and in-plane penetration depth (squares).

oscillations at a natural frequency, $2\pi f_0 = 1/\sqrt{L_0 C}$, where L_0 is the inductance of the coil without a sample inside. The sample, mounted on a sapphire rod, is inserted into the coil without touching it. Because of the diamagnetic susceptibility of the sample, $4\pi\chi = \lambda/R \tanh R/\lambda - 1$, the inductance changes to a new value, L, and the resonant frequency shifts accordingly, $\Delta f = f - f_0 \approx -G4\pi\chi(T)$, where $G = f_0 V_s/2V_c(1-N)$ is the calibration constant, V_s is the sample volume, V_c is the effective coil volume, and N is the demagnetization factor [27]. Throughout the measurement, the circuit is stabilized at 5.0 K $\pm$ 3 mK to ensure a stability in the resonance of less than 0.05 Hz over a period of several hours. The frequency resolution is better than 5 parts in 10^9, which translates into $\sim$1 Å resolution in $\Delta\lambda$ for mm-sized crystals. The sample experiences a $\sim$10 mOe ac excitation field, much smaller than the first critical field, H_{c1}. The calibration constant G has been determined by two different techniques [27,28]. First, the sample was physically pulled from the coil at a low temperature to determine the full frequency change due to its presence. Second, the normal state skin depth was calculated from the measured resistivity just above T_c [Fig. 1(c)]. Both approaches yield the same result, which also rules out inhomogeneity of our samples. The tunnel diode resonator technique precisely measures changes in the penetration depth, but its absolute value is more difficult to obtain [28]. To estimate $\lambda(0)$, we determined H_{c1} by measuring the $M(H)$ loops while increasing the maximum field until nonlinearity due to vortices has appeared. Using $H_{c1} = \Phi_0/(4\pi\lambda^2)(\ln\lambda/\xi + 0.5)$, with a value for the coherence length of $\xi = 2.76$ nm at 6 K measured by scanning tunneling spectroscopy [29], as estimated from the upper critical field, we have obtained $\lambda(0) \approx 208$ nm. This value is similar to other reports, where $\lambda(0) \approx 254$ nm for La-1111 [12] and 190 nm for Sm-1111 [13] from μSR measurements.

The low-temperature behavior of $\Delta\lambda(T) = \lambda(T) - \lambda(0)$ and the superfluid density, $\rho_s(T) \equiv [\lambda(0)/\lambda(T)]^2$, are commonly used to determine the symmetry of the superconducting pairing state [30]. In the case of a fully gapped Fermi surface, $\Delta\lambda(T)/\lambda(0) \approx \sqrt{\pi\Delta(0)/2k_BT} \times \exp[-\Delta(0)/k_BT]$, which is also true for the cases of an anisotropic gap and two-gap superconductivity if one allows $\Delta(0)/T_c$ to be a free parameter. For the isotropic s-wave BCS case, this form is applicable for $T \leq T_c/3$. This is consistent with the data taken in our TDR system for the conventional BCS superconductor Nb (Fig. 2). An s-wave behavior, albeit with an anisotropic gap with a smaller amplitude, is found in $NdFeAsO_{1-x}F_x$ [15] (Fig. 2). In the case of d-wave pairing, $\Delta\lambda(T)/\lambda(0) \approx T[2\ln 2/\alpha\Delta(0)]$, where $\alpha = \Delta^{-1}(0)|d\Delta(\phi)/d\phi|_{\phi\to\phi_{node}}$ [31]. This linear behavior is observed in our measurements

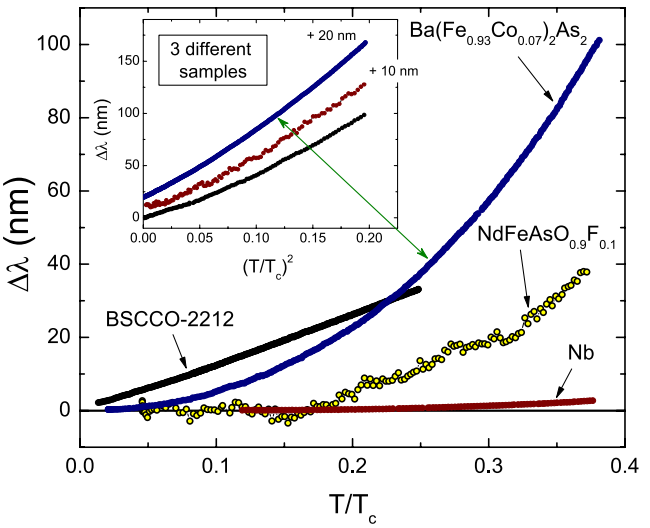

FIG. 2 (color online). Comparison of the low-temperature $\Delta\lambda(T)$ measured in $Ba(Fe_{0.93}Co_{0.07})_2As_2$ with the known d-wave (BSCCO) and s-wave (Nb) superconductors as well as $NdFeAsO_{1-x}F_x$. Inset: $\Delta\lambda$ vs $(T/T_c)^2$ for three different samples of $Ba(Fe_{0.93}Co_{0.07})_2As_2$ from different batches. (Curves are offset for clarity.) Note the slight positive curvature indicating $n > 2$.

on clean BSCCO-2212 crystals (Fig. 2). Impurity scattering does not affect the isotropic s-wave gap, but it does suppress the d-wave gap. The superfluid density, however, does change in both cases, as shown in Fig. 3. In the case of d-wave pairing, scattering leads to $\Delta\lambda(T) \sim T^2$ [17]. For an s-wave superconductor in the dirty limit, $\rho_s(T) = \Delta(T)/\Delta(0)\tanh[\Delta(T)/2k_BT]$ [32].

The observed low-temperature behavior of $\lambda(T)$ in $Ba(Fe_{0.93}Co_{0.07})_2As_2$ is clearly nonexponential (Fig. 2). The inset of Fig. 2 shows the data plotted as a function of $(T/T_c)^2$ for samples from different batches all having different sizes and aspect ratios. The middle curve corresponds to the smallest sample and therefore the smallest filling factor. The fitting of each curve was performed using $\Delta\lambda(T) \sim T^n$. The low-temperature end was fixed at base temperature ($T_{min}/T_c = 0.02$), and the fitting parameters were determined for several values of the high-temperature limit, up to $T_{max}/T_c = 0.4$. This has given values for the exponent n in the range of 2.15 to 2.42. To compare different curves, the fitting range was fixed to $0.3T_c$. This yields $n = 2.4 \pm 0.1$, where the error reflects the scatter of the values of the exponents between different samples. For comparison, the penetration depth for the $NdFeAsO_{1-x}F_x$ crystal, plotted as open circles in Fig. 2, is flat below about $0.2T_c$, providing evidence for a fully gapped Fermi surface [15].

Figure 3 shows $\rho_s(T)$ along with the known s- and d-wave behaviors and the best fit for $NdFeAsO_{1-x}F_x$ [15]. The data for the $Ba(Fe_{0.93}Co_{0.07})_2As_2$ samples are plotted for $\lambda(0) = 200$ nm and 300 nm. The inset of Fig. 3 zooms into the low-temperature region, showing that the observed nonexponential behavior persists down to $0.02T_c$.

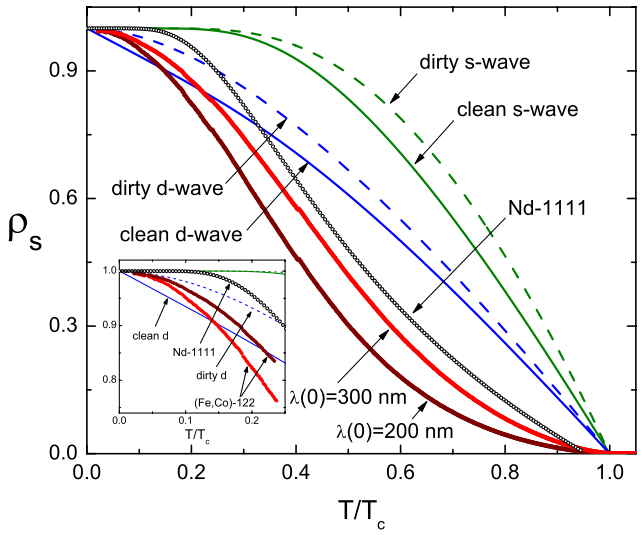

FIG. 3 (color online). Superfluid density, ρ_s, as a function of normalized temperature for $Ba(Fe_{0.93}Co_{0.07})_2As_2$ using $\lambda(0) = 200$ nm and 300 nm. Also shown for comparison are calculated curves for clean and dirty s-wave and d-wave pairings as well as the best fit of the $NdFeAsO_{1-x}F_x$ compound (circles) from Ref. [15].

The value of $\lambda(0) \approx 200$ nm was found from H_{c1} and is consistent with the literature [12,13]. The curve for $\lambda(0) = 300$ nm produces $\rho_s(T)$ closer to the standard curves, but no $\lambda(0)$ can change the nonexponential low-temperature behavior. At intermediate temperatures, the experimental $\rho_s(T)$ shows significant departure from the d-wave and s-wave curves (Fig. 3). This could be due to significant gap anisotropy or multigap pairing with different gap amplitudes.

In clean superconductors the temperature dependence of the penetration depth reflects the superconducting gap topology, with $n = 1$ for line nodes and $n = 2$ for point nodes. Nonlocal effects and impurity scattering act to increase the exponent n [17]. Therefore, possible scenarios to explain the unusual exponent in $\lambda \sim T^n$ depend on whether n is higher or smaller than 2. The exponent $n = 2$ can be explained in a dirty d-wave [17] or gapless state [33]. It can also be explained in an $s_\pm$ pairing model where the scattering from nonmagnetic impurities acts similarly to magnetic impurities in conventional s-wave superconductors, and at high enough impurity scattering rates the superconductor becomes gapless [34–36]. Reasonable fitting of the $\lambda(T)$ curves is possible [35]. Finally, a plausible explanation of the exponent $n > 2$ is the existence of point nodes where a quadratic behavior of $\lambda(T)$ is predicted and observed in the clean case [19,37].

We now turn to compare the 1111 and 122 systems. Both systems share the Fe-As planes as key structural building blocks. Electronic structure calculations demonstrate that the states at the Fermi energy are dominated by Fe-3d states. These two compounds also possess very similar resistivity values. Thus, we discuss our results under the premise that there is a common pairing mechanism and a common pairing symmetry in both materials. Previously, we argued that a likely interpretation of the moderate anisotropy of the superconducting gap, $\Delta(\varphi)$, [9,15] can naturally be understood as a result of an electronic interband $s_\pm$ pairing interaction [36] that changes the sign of the gap. In this scenario, anisotropic s-wave pairing occurs with the nodes located between Fermi surface sheets [38]. If the actual shape of the Fermi surface strongly deviates from cylindrical, the equator of the Fermi surface can reach the points where the OP changes sign and becomes gapless at a single spot. Such an anisotropic s-wave state with nodes implies that the existence of nodes depends sensitively on the Fermi surface shape, in sharp contrast to d- or p-wave states where the nodes are enforced by the symmetry.

Electronic structure calculations were performed within the full-potential linearized plane-wave approach [39] using the local density approximation. Both relaxed and experimental As positions were used with the experimental lattice constants for the $BaFe_2As_2$ [40] and $Ba(Fe_{0.93}Co_{0.07})_2As_2$ (see above). The calculations with relaxed z_{As} give $\gamma_\lambda^2 = \langle v_x^2\rangle/\langle v_z^2\rangle = 3$ for the pure compound and $\gamma_\lambda^2 = 2.7$ for $Ba(Fe_{0.93}Co_{0.07})_2As_2$. With the

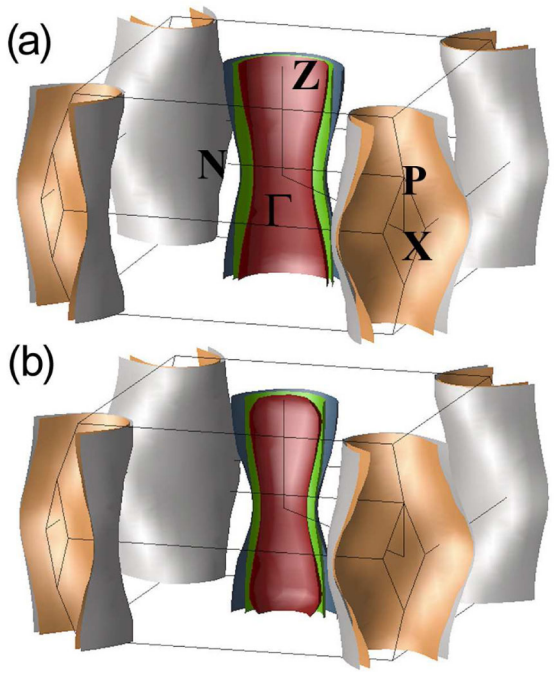

FIG. 4 (color online). (a) Fermi surface of nonsuperconducting (a) $BaFe_2As_2$ and (b) $Ba(Fe_{0.93}Co_{0.07})_2As_2$ with experimental As positions.

experimental z_{As}, the difference is much larger, $\gamma_\lambda^2 = 12.1$ and 9.0, for pure and doped ($x = 0.07$) materials, respectively, as shown in Fig. 4. In either case, the Fermi surface becomes more three dimensional with doping. Actual experimental data for $Ba(Fe_{0.93}Co_{0.07})_2As_2$ estimate γ_λ^2 to be in the range between 4.4 and 6.8 [41], which makes this scenario in principle possible.

In conclusion, a robust power law behavior of the low-temperature penetration depth is found in $Ba(Fe_{0.93}Co_{0.07})_2As_2$ single crystals with $\Delta\lambda \propto T^n$ with $n \approx 2.4 \pm 0.1$. Possible explanations for this unusual exponent require either the existence of gapless regions or point nodes on the Fermi surface in the superconducting state.

We thank A. V. Chubukov, J. R. Clem, A. Kaminski, V. G. Kogan, and I. I. Mazin for discussions and comments. Work at the Ames Laboratory was supported by the Department of Energy–Basic Energy Sciences under Contract No. DE-AC02-07CH11358. R. P. acknowledges support from the Alfred P. Sloan Foundation. M. A. T. acknowledges continuing cross-appointment with the Institute of Surface Chemistry, NAS Ukraine.

Note added in proof.—Recent data on Nd and La 1111 crystals [42] show that the apparent flattening of the penetration depth in Fig. 2 is due to the paramagnetic contribution from Nd ions.

*Corresponding author.
prozorov@ameslab.gov

[1] Y. Kamihara *et al.*, J. Am. Chem. Soc. **130**, 3296 (2008).
[2] Z. A. Ren *et al.*, Chin. Phys. Lett. **25**, 2215 (2008).
[3] For example, D. J. van Harlingen, Rev. Mod. Phys. **67**, 515 (1995); C. C. Tsuei and J. R. Kirtley, Rev. Mod. Phys. **72**, 969 (2000); H. Won *et al.*, Phys. Status Solidi B **242**, 363 (2005).
[4] P. Samuely *et al.*, Supercond. Sci. Technol. **22**, 014 003 (2009).
[5] P. Szabo *et al.*, Phys. Rev. B **79**, 012503 (2009).
[6] T. Y. Chen *et al.*, Nature (London) **453**, 1224 (2008).
[7] G. Mu *et al.*, arXiv:0808.2941.
[8] G. Mu *et al.*, Chin. Phys. Lett. **25**, 2221 (2008).
[9] Chang Liu *et al.*, arXiv:0806.2147.
[10] D. V. Evtushinsky *et al.*, Phys. Rev. B **79**, 054517 (2009).
[11] K. Hashimoto *et al.*, Phys. Rev. Lett. **102**, 017002 (2009).
[12] H. Luetkens *et al.*, Phys. Rev. Lett. **101**, 097009 (2008).
[13] A. Drew *et al.*, Phys. Rev. Lett. **101**, 097010 (2008).
[14] L. Malone *et al.*, arXiv:0806.3908.
[15] R. Prozorov *et al.*, Physica C (Amsterdam) (to be published).
[16] R. Prozorov *et al.*, Phys. Rev. Lett. **85**, 3700 (2000).
[17] P. J. Hirschfeld and N. D. Goldenfeld, Phys. Rev. B **48**, R4219 (1993).
[18] K. Izawa *et al.*, Phys. Rev. Lett. **90**, 117001 (2003).
[19] E. E. M. Chia *et al.*, Phys. Rev. Lett. **91**, 247003 (2003).
[20] K. Izawa *et al.*, Phys. Rev. Lett. **89**, 137006 (2002).
[21] A. Sefat *et al.*, Phys. Rev. Lett. **101**, 117004 (2008).
[22] A. Yamamoto *et al.*, Appl. Phys. Lett. **94**, 062 511 (2009).
[23] R. Prozorov *et al.*, Phys. Rev. B **78**, 224506 (2008).
[24] N. Ni *et al.*, Phys. Rev. B **78**, 014507 (2008).
[25] N. Ni *et al.*, Phys. Rev. B **78**, 214515 (2008).
[26] C. T. Van Degrift, Rev. Sci. Instrum. **46**, 599 (1975).
[27] R. Prozorov *et al.*, Phys. Rev. B **62**, 115 (2000).
[28] R. Prozorov *et al.*, Appl. Phys. Lett. **77**, 4202 (2000).
[29] Y. Yin *et al.*, Phys. Rev. Lett. **102**, 097002 (2009).
[30] R. Prozorov and R. W. Giannetta, Supercond. Sci. Technol. **19**, R41 (2006).
[31] D. Xu, S. K. Yip, and J. A. Sauls, Phys. Rev. B **51**, 16 233 (1995).
[32] M. Tinkham, *Introduction to Superconductivity* (Dover, New York, 1996), 2nd ed..
[33] V. G. Kogan *et al.*, J. Phys. Condens. Matter **21**, 102 204 (2009).
[34] A. V. Chubukov *et al.*, Phys. Rev. B **78**, 134512 (2008); D. Parker *et al.*, Phys. Rev. B **78**, 134524 (2008).
[35] A. B. Vorontsov *et al.*, arXiv:0901.0719.
[36] I. I. Mazin *et al.*, Phys. Rev. Lett. **101**, 057003 (2008).
[37] D. Einzel *et al.*, Phys. Rev. Lett. **56**, 2513 (1986).
[38] R. Sknepnek *et al.*, Phys. Rev. B **79**, 054511 (2009).
[39] P. Blaha *et al.*, in *An Augmented Plane Wave + Local Orbitals Program for Calculating Crystal Properties*, edited by K. Schwarz (TU Wien, Vienna, 2001).
[40] M. Rotter, M. Tegel, and D. Johrendt, Phys. Rev. Lett. **101**, 107006 (2008).
[41] M. A. Tanatar *et al.*, Phys. Rev. B **79**, 094507 (2009).
[42] C. Martin *et al.*, arXiv:0903.2220.